ISOTHERMAL SECTION OF THE La₂O₃-Lu₂O₃-Er₂O₃ TERNARY PHASE DIAGRAM AT 1250°C

Olga Chudinovych [a,b]

*ᵃFrantsevich Institute for Problems in Materials Science NAS of Ukraine,
3, Krzhizhanovsky str., Kyiv 03142, Ukraine*
*ᵇNational Technical University of Ukraine "Igor Sikorsky Kyiv Polytechnic Institute",
4, Peremohy ave., Kyiv 03050, Ukraine*
e-mail: chudinovych_olia@ukr.net

Abstract. The phase equilibria in the ternary La₂O₃–Lu₂O₃–Er₂O₃ system at 1250°C were studied by X-ray diffraction, and electron microscopy in the overall concentration range. At 1250°C in the La₂O₃–Lu₂O₃–Er₂O₃ system solution fields are formed based on cubic (C) modification of Lu₂O₃(Er₂O₃), hexagonal (A) modification of La₂O₃, as well as ordered phase structure perovskite-type LaLuO₃ (LaErO₃) (R). The isothermal section of the La₂O₃–Lu₂O₃–Er₂O₃ phase diagram at 1250°C has shown the three one-phase fields (A-La₂O₃, R, C-Lu₂O₃(Er₂O₃)) corresponding to solid solutions based on starting components and two dual-phase fields (C+R, A+R) between them. The refined lattice parameters of the unit cells for solid solutions and microstructures of the definite field of compositions for the systems solid were determined.

Keywords: phase equilibria, lanthana, lutetia, erbia, lattice parameter.

Introduction

The oxides of rare earth elements (REE) have unique properties (fire resistance, corrosion resistance, high thermomechanical and electrical characteristics, *etc*.). Due to this, they have a wide range of uses. Materials based on solid solutions of rare earth elements are used in electronics, optoelectronics, mechanical engineering, chemical industry, metallurgy, medicine, laser development, *etc*. [1-6]. The system containing oxides of lanthanum, lutetium, and erbium are promising in terms of the development of optically transparent ceramics.

State diagrams based on La₂O₃–Lu₂O₃–Ln₂O₃ are a physicochemical basis for the development of various functional materials. Recently, ternary oxides containing rare earth elements have attracted attention as alternative dielectrics [2-9]. One of the materials of this class is LaLuO₃, which has a high relative permittivity k in the range from 20 to 32, a band gap of 5.6 ēV, symmetric band shifts to silicon of 2.1 ēV, and was characterized by high thermal stability. Generally, ternary oxides exhibit higher permittivity compared to the corresponding binary oxides without decreasing the band gap, making LaLuO₃ more promising than La₂O₃ or Lu₂O₃. Of special interest are thin orthorhombic LaLuO₃

films, which can have k (relative permittivity) even higher than 40 [7-9]. Compounds based on rare earth element oxides were used to produce lasers and other optically active elements in optoelectronics [4-6].

However, information on phase equilibria in the ternary La₂O₃-Lu₂O₃-Ln₂O₃ systems is absent and requires further research. Previously, systems based on La₂O₃–Y₂O₃–Ln₂O₃ (Ln= Nd, Sm, Gd, Yb, Er) [10-12] and La₂O₃–Lu₂O₃–Yb₂O₃ [13,14] have been investigated.

The phase relations and structures of the phases formed in the La₂O₃–Er₂O₃ system were examined previously [15-23], revealing that there are solid solutions of cubic (C) and hexagonal (H) Er₂O₃ modifications and low-temperature hexagonal (A) and high-temperature hexagonal (H), cubic (X) La₂O₃ modifications and ordered phase structure perovskite-type LaErO₃. The La₂O₃–Er₂O₃ system at 1100°C (and at 1500°C) is characterized by the hexagonal (A) modification of lanthanum oxide with the solubility of Er₂O₃ 5 mol% (and 13 mol% at 1500°C), cubic (C) modification of erbium oxide with the solubility of A-La₂O₃ ~6 mol% (and ~11 mol% at 1500°C), and ordered perovskite-type LaErO₃ (R) phase in the range 45–51 mol% Er₂O₃ (and 45-51 mol% Er₂O₃ at

1500°C) [16]. The phase relations and structures of the phases formed in the La_2O_3–Lu_2O_3 system have been investigated [15,24,25]. The melt was crystallized at temperatures above 2000°C to obtain perovskite-like $LaLuO_3$ single crystals, the orthorhombic cell parameters are *a*= 6.00 nm, *b*= 5.79 nm, *c*= 8.35 nm and the space group is *Pnam* [15]. Calculations of oxygen vacancies in La_2O_3, Lu_2O_3, and $LaLuO_3$ have been also provided previously [24], but there were no data on phase equilibria (Figure 1).

The phase diagrams of the system consisting of oxides at the end of the lanthanide series feature infinite solid solutions based on A, B, C, H, and X modifications of REE oxides [22,26-29]. Phase equilibria in binary systems based on oxides of rare earth elements have been studied completely. However, information on phase equilibria in the ternary La_2O_3-Lu_2O_3-Er_2O_3 system is absent and requires further research.

The purpose of this work was to study the interaction of lanthanum, lutetium and erbium oxides at 1250°C in the entire concentration range and to construct the corresponding isothermal section of the phase diagram.

Experimental
Materials
The starting materials were Lu_2O_3, La_2O_3, and Er_2O_3 (produced by Merck company) with 99.99% of the main component and analytical-grade nitric acid.

Instruments
The samples were subjected to *X-ray powder diffraction* technique using a DRON-3 diffractometer at room temperature (Cu-K_α radiation λ= 1.5418 Å). The voltage on the X-ray tube was 30 kV, and the current was 20 mA. The scan angle was 0.05–0.1 in the range 2θ= 15–80°. The lattice parameters were calculated with the least-square method employing the LATTIC software [30], with an error of less than 0.0002 nm for the cubic phase. The phase composition was determined of the Joint Committee on Powder Diffraction Standards (JCPDS International Center for Diffraction Data, 1999).

The microstructures of the samples were studied by *scanning electron microscopy* with a Superprobe-733 analyzer (JEOL, Japan) in back-scattered electrons (BSE) and secondary electrons (SE) (×400, ×2000).

(a)

(b)
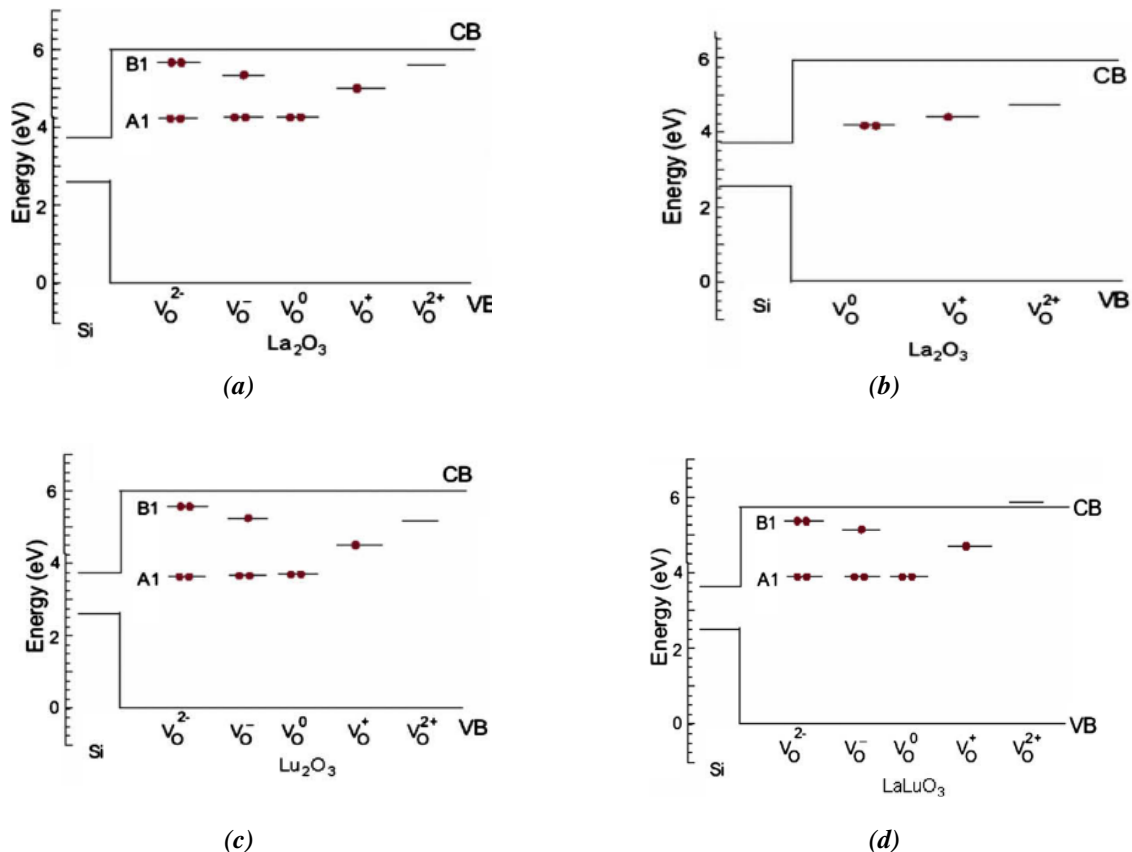

(c)

(d)

Figure 1. Energy levels of fourfold coordinated O vacancy in La_2O_3 *(a)* and *(b)*, Lu_2O_3 *(c)*, and $LaLuO_3$ *(d)*.

Synthesis of the samples

The samples were prepared with a concentration step of 1–5 mol%. Weighed oxide portions were dissolved in HNO_3 (1:1) and then the solutions were evaporated and the nitrates decomposed into oxides by calcination at 800°C for 2 h. The powders were pressed as pellets 5 mm in diameter and 4 mm in height at 10 MPa. The samples were heat treated in a furnace with H23U5T (FeCrAl alloy) heating elements at 1250°C in air.

Results and discussion

Compositions of the investigated samples fall into two beams: Lu_2O_3 – (50 mol% La_2O_3 – 50 mol% Er_2O_3) and La_2O_3 – (50 mol% Lu_2O_3 – 50 mol% Er_2O_3). Chemical and phase compositions of the samples annealed at 1250°C and the lattice parameters of the phases that are in equilibrium at this temperature are summarized in Table 1. The results were used to construct the isothermal section of the La_2O_3–Lu_2O_3–Er_2O_3 phase diagram at 1250°C (Figure 2).

Table 1

Phase composition and lattice parameters of the phases in the La_2O_3–Lu_2O_3–Er_2O_3 samples, annealed at 1250°C.

Chemical composition (mol%)			Phases by XRD	Lattice parameters of the phases $\sigma\pm0.0002$ (nm)					
				R			<C>	<A>	
Lu_2O_3	La_2O_3	Er_2O_3		a	b	c	a	a	c
Section Lu_2O_3 — (50 mol% La_2O_3 — 50 mol% Er_2O_3)									
0	50	50	R+<C>traces	0.607	0.588	0.847			
1	49.5	49.5	R+<C>traces	0.608	0.586	0.846			
2	49	49	R+<C>	0.608	0.584	0.844	1.054		
3	48.5	48.5	R+<C>	0.607	0.587	0.847	1.049		
4	48	48	R+<C>	0.607	0.587	0.846	1.062		
5	47.5	47.5	R+<C>	0.608	0.586	0.845	1.048		
10	45	45	R+<C>	0.606	0.586	0.847	1.058		
15	42.5	42.5	R+<C>	0.607	0.586	0.845	1.051		
20	40	40	R+<C>	0.609	0.584	0.845	1.054		
30	35	35	R+<C>	0.608	0.582	0.850	1.053		
70	15	15	R+<C>	0.603	0.580	0.843	1.045		
80	10	10	Rtraces+<C>				1.043		
85	7.5	7.5	Rtraces+<C>				1.043		
90	5	5	Rtraces+<C>				1.043		
95	2.5	2.5	<C>				1.043		
100	0	0	<C>	—	—	—	1.039		
Section La_2O_3 — (50 mol % Lu_2O_3 — 50 mol % Er_2O_3)									
50	0	50	<C>				1.050		
49	2	49	<C>				1.050		
48	4	48	<C>+ Rtraces				1.051		
47.5	5	47.5	<C>+ Rtraces				1.051		
45	10	45	<C>+ Rtraces				1.050		
30	40	30	R+<C>	0.606	0.584	0.843	1.052		
29	42	29	R+<C>	0.607	0.583	0.842	1.052		
27.5	45	27.5	R+<C>	0.607	0.584	0.842	1.051		
26	48	26	R+<C>	0.604	0.584	0.842	1.050		
25	50	25	R+<C>traces	0.605	0.584	0.842			
23.5	53	23.5	R	0.606	0.584	0.844			
22.5	55	22.5	<A>+ R	0.603	0.585	0.845		0.658	0.381
20	60	20	<A>+ R	0.605	0.587	0.845		0.657	0.382
7.5	85	7.5	<A> + R	0.605	0.584	0.844		0.653	0.384
5	90	5	<A>+ R	0.607	0.582	0.842		0.654	0.384
4	92	4	<A>+ R	0.605	0.583	0.843		0.655	0.384
2.5	95	2.5	<A>+ R	0.605	0.584	0.845		0.654	0.385
0	100	0	<A>					0.652	0.386

Note that the oxide of lanthanum is subject to hydration in air and, thus, instead of hexagonal A-La_2O_3 in the samples after heat treatment at 1250°C we found the formation of hexagonal A-$La(OH)_3$. This arose in the presented work, however, proper storage and prompt investigation after annealing would have made it possible to obtain A-La_2O_3. Nevertheless, since this applies only to A-La_2O_3 in the investigated system, the results obtained for $La(OH)_3$ can be attributed to A-La_2O_3. Designation of phases: <A> - solid solutions based on hexagonal modifications of $La(OH)_3$; <C> - solid solutions based on cubic modification of $Lu_2O_3(Er_2O_3)$; R – ordered phase of $LaLuO_3(LaErO_3)$ with perovskite-type structure with rhombic distortions.

At 1250°C in the La_2O_3–Lu_2O_3–Er_2O_3 system solution fields are formed based on cubic (C) modification of $Lu_2O_3(Er_2O_3)$, hexagonal (A) modification of La_2O_3, as well as ordered phase structure perovskite-type $LaLuO_3$ $(LaErO_3)(R)$. No new phases were found. An infinite continuous series of solid solutions based on ordered perovskite-type phases forms in the La_2O_3–Lu_2O_3–Er_2O_3 system. This indicates the mutual substitution of $Lu^{3+}(r= 0.085$ nm) ions by $Er^{3+}(r= 0.0881$ nm), and vice versa. The homogeneity range of the R-phase extends in compliance with its solubility limits in the boundary binary La_2O_3–Lu_2O_3 and La_2O_3–Er_2O_3 systems. Using the concentration dependences of the unit cell parameters, it was established that the range of homogeneity of solid solutions based on the R-phase extends from 51 to 54 mol% La_2O_3 at 1250°C in the section La_2O_3 – (50 mol% Lu_2O_3 – 50 mol% Er_2O_3) (Figure 3). The lattice parameters of the unit cell R-phase vary from $a= 0.606$ nm, $b= 0.584$ nm, $c= 0.842$ nm in single-phase sample, containing 23.5 mol% Lu_2O_3–53 mol% La_2O_3–23.5 mol% Er_2O_3 to $a= 0.603$ nm, $b= 0.585$ nm, $c= 0.845$ nm in two-phase sample (R +A), containing 22.5 mol% Lu_2O_3–55 mol% La_2O_3–22.5 mol% Er_2O_3.

Similar to this system, in the La_2O_3–Lu_2O_3–Yb_2O_3 [14] and La_2O_3–Y_2O_3–Er_2O_3 [31] systems at 1500°C, continuous series of solid solutions based on an ordered phase with a perovskite-type structure are also formed. In contrast, in the La_2O_3–Y_2O_3–Nd_2O_3 system at 1500°C, a region of solid solutions is formed based on an ordered phase with a perovskite-type structure. The maximum solubility of neodymium oxide in the R-phase is ~7 mol% along section Nd_2O_3– (50 mol% La_2O_3-50 mol% Y_2O_3) [10].

Lutetium and erbium oxides form series of C-REE oxide solid solutions. This field ranges along the Lu_2O_3–Er_2O_3 side of the composition triangle. The homogeneity range of the C-phase extends in compliance with its solubility limits in the boundary binary La_2O_3–Lu_2O_3, La_2O_3–Er_2O_3 and Lu_2O_3–Er_2O_3 systems. This direction of the homogeneity range of the C-phase indicates that Lu^{3+} ions are predominantly replaced by Er^{3+} ions and *vice versa*, without charge compensation. Using the concentration dependences of the unit cell parameters, it was established that the range of homogeneity of solid solutions based on the C-phase extends from 93 to 100 mol% Lu_2O_3 at 1250°C in the section Lu_2O_3 – (50 mol% La_2O_3 – 50 mol% Er_2O_3) (Figure 4).

○ — single-phase and ◐- two-phase regions
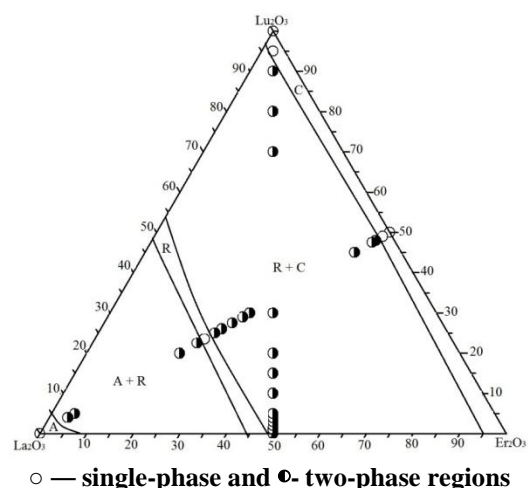
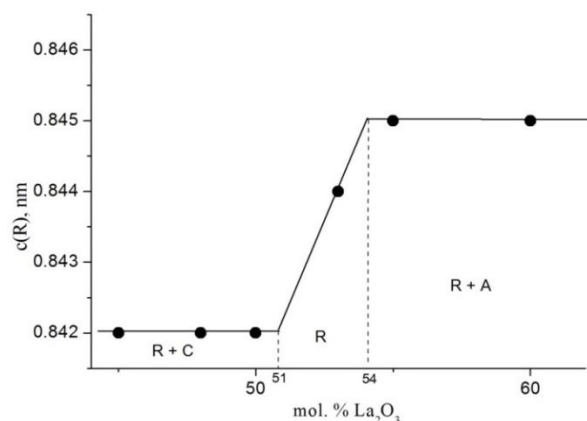**Figure 2. The isothermal section of the La_2O_3–Lu_2O_3–Er_2O_3 phase diagram at 1250°C.**

Figure 3. Concentration dependence of lattice parameters *c* for R-based solid solutions annealed at 1250°C along the section La_2O_3 – (50 mol% Lu_2O_3 – 50 mol% Er_2O_3) in the system La_2O_3–Lu_2O_3–Er_2O_3.
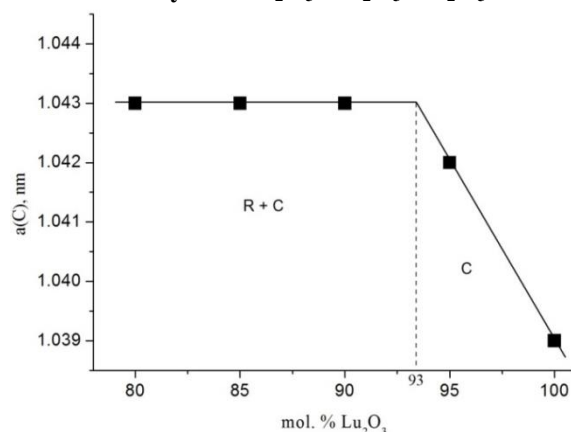

Figure 4. Concentration dependence of lattice parameters *a* for C-based solid solutions annealed at 1250°C along the section Lu_2O_3 – (50 mol% La_2O_3 – 50 mol% Er_2O_3) in the system La_2O_3–Lu_2O_3–Er_2O_3.

The lattice parameters of the unit cell C-phase vary from $a= 1.050$ nm in single-phase sample, containing 49 mol% Lu_2O_3 − 2 mol% La_2O_3 − 49 mol% Er_2O_3 to $a= 1.052$ nm in two-phase sample (C+R), containing 30 mol% Lu_2O_3 − 40 mol% La_2O_3 − 30 mol% Er_2O_3. The X-ray diffraction patterns for the samples that characterize the phase field in the La_2O_3–Lu_2O_3–Er_2O_3 system at 1250°C are presented in Figure 5. In the region with a high content of La_2O_3 solid solutions are formed based on the hexagonal modification of lanthanum oxide. The homogeneity range of the solid solution based on the hexagonal (A) modification of lanthanum oxide is not extensive wide. Note that the oxide of lanthanum in the air is subject to hydrating and thus, instead of hexagonal phase La_2O_3 in samples at 1250°C we find the formation of hexagonal hydroxide of $La(OH)_3$ (Figure 4(d) and (e)). Nevertheless, since this applies only to A-La_2O_3 in the investigated system, the results obtained for $La(OH)_3$ can be attributed to A-La_2O_3.

Using the concentration dependences of the unit cell parameters, it was established that the range of homogeneity of solid solutions based on the A-phase extends from 96 to 100 mol% La_2O_3 at 1250°C in the section La_2O_3 − (50 mol% Lu_2O_3 − 50 mol% Er_2O_3) (Figure 6).

The lattice parameters of the unit cell A-phase varies from $a= 0.652$ nm, $c= 0.386$ nm in single-phase sample, containing 0 mol% Lu_2O_3 − 100 mol% La_2O_3 − 0 mol% Er_2O_3 to $a= 0.655$ nm, $c= 0.384$ nm in two-phase sample (A+R), containing 4 mol% Lu_2O_3 − 92 mol% La_2O_3 − 4 mol% Er_2O_3.

Depending on the lutetium oxide content, microstructural changes in the two-phase samples (C + R) can be followed in Figure 7. The light phase is C, and the dark phase is R. The results of the microprobe X-ray analysis of the two-phase sample (C+R), containing 3 mol% Lu_2O_3 − 48.5 mol% La_2O_3 − 48.5 mol% Er_2O_3 confirmed the presence of two phases (Table 2). In the sample containing 3 mol% Lu_2O_3 − 48.5 mol% La_2O_3 − 48.5 mol% Er_2O_3, the dark phase is the matrix one (Figure 8). The quantitative analysis of elements in local points (R1-R5) in the main dark phase showed that it contains La ~31 at% and almost the same Er ~31 at%. Hence it is the R-phase. The quantitative analysis of elements in local points (S1-S5) of the light phase showed, that it contains significantly more Er ~57 at% and

significantly less La (~6 at%) and Lu (~2 at%) (Table 2). Therefore, the light phase may be identified C-Er_2O_3. Black areas are pores. Other samples have the same phase by contrast, so elemental composition was not carried out for them.
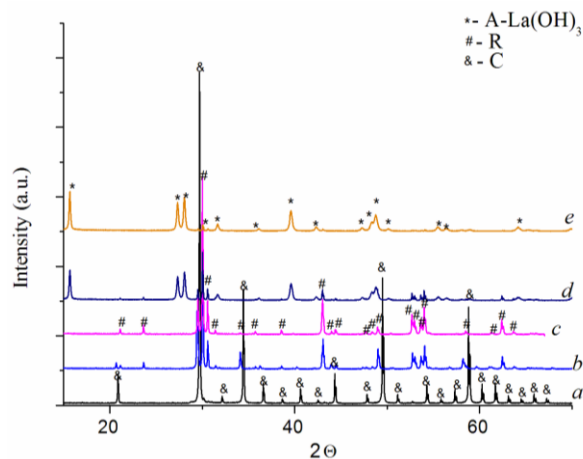

Figure 5. XRD patterns from the La_2O_3–Lu_2O_3–Er_2O_3 samples heat-treated at 1250°C. (49 mol% Lu_2O_3 − 2 mol% La_2O_3 − 2 mol% Er_2O_3 (C, (CCC, Ia3)) (a); 30 mol% Lu_2O_3–40 mol% La_2O_3 − 30 mol% Er_2O_3 (C(CCC, Ia3)+R(Primitive, Pnam) (b); 23.5 mol% Lu_2O_3–53 mol% La_2O_3–23.5 mol% Er_2O_3 (R((Primitive, *Pnam*)) (c); 5 mol% Lu_2O_3 − 90 mol% La_2O_3 − 5 mol% Er_2O_3 (R((Primitive, *Pnam*)+A(Primitive, P63/m) (d); 0 mol% Lu_2O_3 − 100 mol% La_2O_3 − 0 mol% Er_2O_3 (A(Primitive, P63/m)) (e)).

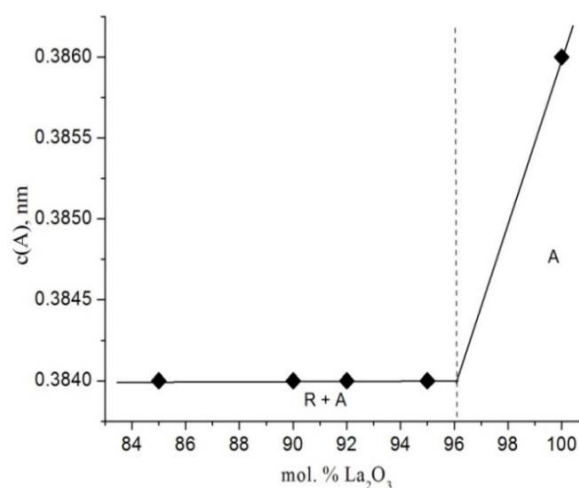**Figure 6. Concentration dependence of lattice parameters c for solid solutions based on A-$La(OH)_3$ heat-treated at 1250°C along the section of La_2O_3 − (50 mol% Lu_2O_3 − 50 mol% Er_2O_3) in the system La_2O_3–Lu_2O_3–Er_2O_3.**
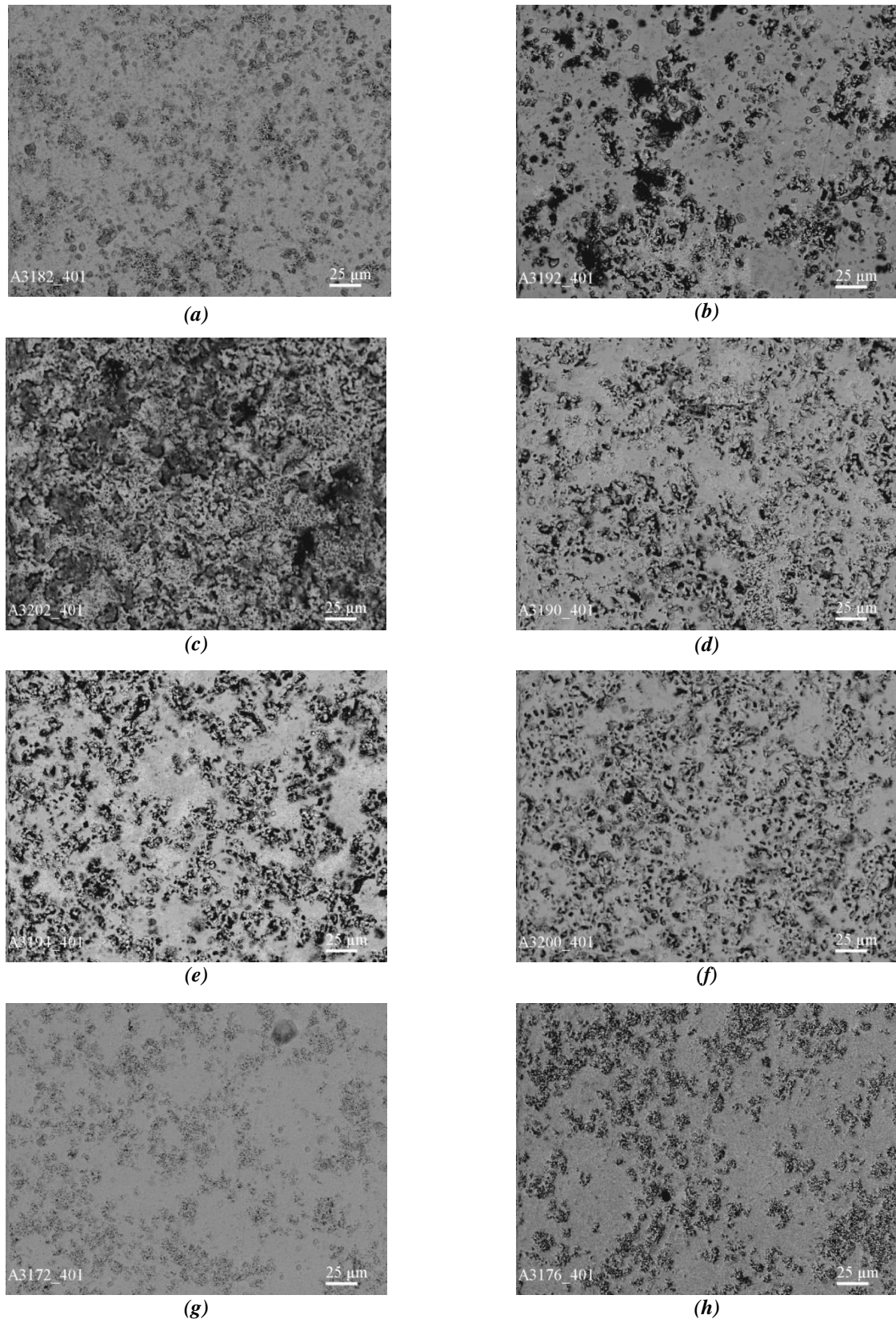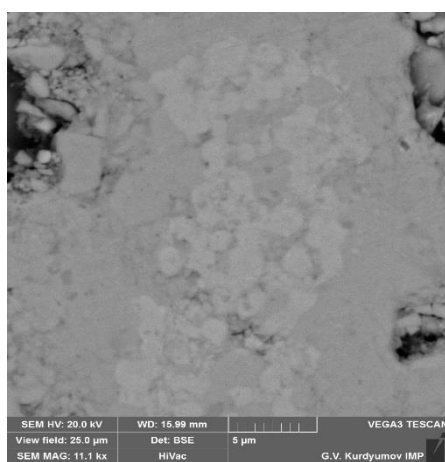
Figure 7. SEM microstructures of the samples heat-treated at 1250°C in the definite field of compositions of the system La$_2$O$_3$–Lu$_2$O$_3$–Er$_2$O$_3$, BSE×400.
(5 mol% La$_2$O$_3$ – 47.5 mol% Lu$_2$O$_3$ – 47.5 mol% Er$_2$O$_3$ (R+C) *(a)*; 50 mol% La$_2$O$_3$ - 0 mol% Lu$_2$O$_3$ - 50 mol% Er$_2$O$_3$(R+C) *(b)*; 49 mol% La$_2$O$_3$ – 2 mol% Lu$_2$O$_3$ - 49 mol% Er$_2$O$_3$(R+C) *(c)*; 48.5 mol% La$_2$O$_3$ – 3 mol% Lu$_2$O$_3$ - 48.5 mol% Er$_2$O$_3$(R+C) *(d)*; 48 mol% La$_2$O$_3$ – 4 mol% Lu$_2$O$_3$ – 48 mol% Er$_2$O$_3$(R+C) *(e)*;47.5 mol% La$_2$O$_3$ – 5 mol% Lu$_2$O$_3$ – 47.5 mol% Er$_2$O$_3$(R+C) *(f)*; 42.5 mol% La$_2$O$_3$ –15 mol% Lu$_2$O$_3$ – 42.5 mol% Er$_2$O$_3$(R+C) *(g)*; 0 mol% La$_2$O$_3$ –50 mol% Lu$_2$O$_3$ – 50 mol% Er$_2$O$_3$(C) *(h)*).

Composition of the phases in the samples, annealed at 1250°C in air (EDX data).

Chemical composition (mol %)				Elemental composition (at%)				
La₂O₃	Lu₂O₃	Er₂O₃	Spectrum	O	La	Er	Lu	Total
48.5	3	48.5	S1	34.92	6.24	56.94	1.90	100.0
			S2	34.82	6.86	56.31	2.01	100.0
			S3	34.38	5.87	57.93	1.83	100.0
			S4	33.87	4.92	59.90	1.31	100.0
			S5	35.72	6.40	55.87	2.01	100.0
			R1	37.36	30.40	30.74	1.50	100.0
			R2	37.63	30.49	27.85	4.04	100.0
			R3	35.87	30.39	32.25	1.49	100.0
			R4	36.23	31.37	30.92	1.48	100.0
			R5	33.69	32.19	32.69	1.43	100.0

(a)
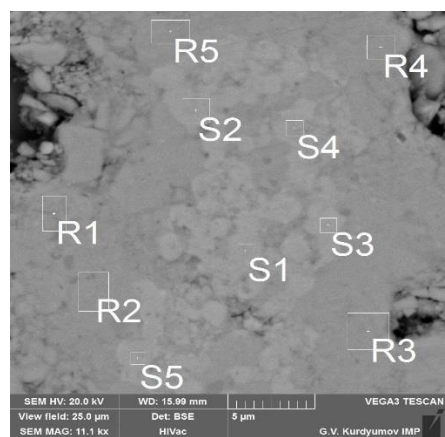
(b)

Figure 8. SEM microstructures of the sample heat-treated at 1250°C in the system La₂O₃–Lu₂O₃–Er₂O₃ 48.5 mol% La₂O₃ – 3 mol% Lu₂O₃ - 48.5 mol% Er₂O₃(R+C) light grains - <C-Er₂O₃>, dark grains – R, black - pores.

The difference between the unit cell volumes of the orthorhombic phase R (0.298 nm^3) and C-cubic solid solution (1.157 nm^3) is big enough so that the large La^{3+} (0.114 nm) ions easily replace small ions of Er^{3+} (0.088 nm) (Lu^{3+} (0.085 nm)) in the lattice of C-phase solid

solution. The substitution of Er^{3+}(Lu^{3+}) ions by La^{3+} ion is accompanied by phase transition (C→R) and shrinkage of the volume and pores formation. The substitution is accompanied by shrinkage of the samples due to the ordering of initially disordered C-solid solution. Ordering of the R-phase is a diffusion-controlled process carried out gradually. Before ordering sintering and densification to high relative density takes place. Then dense ceramics transforms to the ordered R-phase. As a result, numerous pores formed and located at the grain boundaries between the grains of the light gray C-phase of the disordered solid solution and dark gray grains of the ordered R-phase. The light gray phase is near pores, whereas the dark gray phase comprises pores of different sizes. The two-phase solid solution based on C-phase and R-phase is randomly mixed, and in this case, the porosity is low.

Conclusions

Phase equilibria have been studied in the La₂O₃–Lu₂O₃–Er₂O₃ system at 1250°C. It has been established that solid state interactions between three oxides resulted in the formation of extended fields of solid solutions based on various crystal modifications of the initial components of rare-earth oxides, as well as the ordered phase of perovskite type.

The continuous series area of solid solutions based on ordered perovskite-type phases forms in the La₂O₃–Lu₂O₃–Er₂O₃ system. The isothermal section of the La₂O₃–Lu₂O₃–Er₂O₃ phase diagram at 1250°C has characterized the three one-phase fields (A-La₂O₃, R, C-Lu₂O₃(Er₂O₃)) corresponding to solid solutions based on starting components and two two-phase fields (C-Lu₂O₃(Er₂O₃)+R, A-La₂O₃+R) between them. According to the obtained results, no new phases were found.

References

1. Zhu, B.; Ohno, H.; Kosugi, S.; Hori, F.; Yasunaga, K.; Ishikawa, N.; Iwase, A. Effects of swift heavy ion irradiation on the structure of Er_2O_3-doped CeO_2. Nuclear Instruments and Methods in Physics Research, 2010, 268(19), pp. 3199–3202.
DOI: https://doi.org/10.1016/j.nimb.2010.05.088

2. Montini, T.; Milchionna, M.; Monai, M.; Fornasiero, P. Fundamentals and catalytic applications of CeO_2-Based materials. Chemical Reviews, 2016, 116(10), pp. 5987–6041.
DOI: https://doi.org/10.1021/acs.chemrev.5b00603

3. Wang, J.; Xiao, X.; Liu, Y.; Pan, K.; Pang, H.; Wei, S. The application of CeO_2-based materials in electrocatalysis. Journal of Materials Chemistry A, 2019, 7(30), pp. 17675–17702.
DOI: https://doi.org/10.1039/C9TA04804A

4. Chen, S.; Wu, Y. New opportunities for transparent ceramics. American Ceramic Society Bulletin, 2013, 92(2), pp. 32–37.
https://bulletin-archive.ceramics.org/is-cacheable/1605850390595/ucujnk.pdf

5. Akiyama, J.; Sato, Y.; Taira, T. Laser ceramics with rare-earth-doped anisotropic materials. Optics Letters, 2010, 35(21), pp. 3598–3600.
DOI: https://doi.org/10.1364/OL.35.003598

6. Sanghera, J.; Kim, W.; Villalobos, G.; Shaw, B.; Baker, C.; Frantz, J.; Sadowski, B.; Aggarwal, I. Ceramic laser materials. Materials, 2012, 5(2), pp. 258–277.
DOI: https://doi.org/10.3390/ma5020258

7. Lehmann, J.; Shevchenko, N.; Mucklich, A.; Borany, J.V.; Skorupa, W.; Schubert, J.; Lopez, J.M.J.; Mantl, S. Millisecond flash-lamp annealing of $LaLuO_3$. Microelectronic Engineering, 2011, 88(7), pp. 1346–1348.
DOI: https://doi.org/10.1016/j.mee.2011.03.126

8. Kopia, A.; Kowalski, K.; Leroux, Ch.; Gavarri, J.R. Influence of the substrate on the structure stability $LaLuO_3$ thin films deposited by PLD method. Vacuum, 2016, 134, pp. 120–129.
DOI: https://doi.org/10.1016/j.vacuum.2016.10.005

9. Tryus, M.; Nikolaev, K.V.; Makhotkin, I.A.; Schubert, J.; Kibkalo, L.; Danylyuk, S.; Giglia, A.; Nicolosi, P.; Juschkin, L. Optical and structural characterization of orthorhombic $LaLuO_3$ using extreme ultraviolet reflectometry. Thin Solid Films, 2019, 680, pp. 94-101.
DOI: https://doi.org/10.1016/j.tsf.2019.04.037

10. Chudinovych, O.V.; Andrievskaya, O.R.; Bogatyryova, J.D.; Kovylyaev, V.V.; Bykov, O.I. Phase equilibria in the La_2O_3-Y_2O_3-Nd_2O_3 system at 1500°C. Journal of the European Ceramic Society, 2021, 41(13), pp. 6606–6616. DOI: https://doi.org/10.1016/j.jeurceramsoc.2021.06.017

11. Chudinovych, O.V.; Bykov, O.I.; Samelyuk. A.V. Phase equilibria in the La_2O_3-Y_2O_3-Gd_2O_3 system at 1500 C. Processing and Application of Ceramics, 2022, 16(4), pp. 328–334.
DOI: https://doi.org/10.2298/PAC2204328C

12. Chudinovych, O.V.; Korichev, S.F.; Andrievskaya, O.R. Interaction of yttrium, lanthanum, and samarium oxides at 1600°C. Powder Metallurgy and Metal Ceramics, 2020, 58(9), pp. 599–607.
DOI: https://doi.org/10.1007/s11106-020-00113-0

13. Chudinovych, O.V.; Bykov, O.I.; Sameliuk, A.V. Interaction of lanthanum, lutetium, and ytterbium oxides at 1600°C. Powder Metallurgy and Metal Ceramics, 2021, 60(5-6), pp. 337–345.
DOI: https://doi.org/10.1007/s11106-021-00248-8

14. Chudinovych, O.V.; Bykov, O.I.; Samelyuk, A.V. Phase relation studies in the La_2O_3–Lu_2O_3–Yb_2O_3 system at 1500°C. Journal of Chemistry and Technologies, 2021, 29(4), pp. 485–494. DOI: https://doi.org/10.15421/jchemtech.v29i4.238943

15. Müller-Buschbaum, Hk.; Graebner, P.H. Zur kristallstruktur von $LaErO_3$ und $LaLuO_3$. Zeitschrift für anorganische und allgemeine Chemie, 1971, 386(2), pp. 158–162.
DOI: https://doi.org/10.1002/zaac.19713860205

16. Kornienko, O.A.; Chudinovych, O.V.; Bykov, O.I.; Samelyuk, A.V.; Andrievskaya, E.R. Phase equilibria in the La_2O_3–Er_2O_3 system in the temperature range 1100–1500°C. Powder Metallurgy and Metal Ceramics, 2019, 58(1-2), pp. 89–98.
DOI: https://doi.org/10.1007/s11106-019-00051-6

17. Schneider, S.J.; Roth, R.S. Phase equilibria in systems involving the rare-earth oxides. Part II: Solid state reactions in trivalent rare-earth oxide systems. Journal of Research of the National Bureau of Standards, 1960, 64A(4), pp. 317–332.
DOI: https://doi.org/10.6028/jres.064A.031

18. Foex, M.; Traverse, J.P. Study of the polymorphism of rare earth sesquioxides at high temperature. Mineralogy Bulletin, 1966, 89(2), pp. 184–205. (in French).
DOI: https://doi.org/10.3406/bulmi.1966.5951

19. Coutures, J.; Rouanet, A.; Verges, R.; Foex, M. High temperature study of systems formed by lanthanum sesquioxide and lanthanide sesquioxides. I. Phase diagrams (1400°C < T < T Liquid). Journal of Solid State Chemistry, 1976, 17(1-2), pp. 172–182. (in French). DOI: https://doi.org/10.1016/0022-4596(76)90218-8

20. Zinkevich, M. Thermodynamics of rare earth sesquioxides. Progress in Materials Science, 2007, 52(4), pp. 597–647.
DOI: https://doi.org/10.1016/j.pmatsci.2006.09.002

21. Zhang, Y. Thermodynamic Properties of Rare Earth Sesquioxides. McGill University, Montreal, QC, Canada, 2016, 151 p.
https://escholarship.mcgill.ca/downloads/b2773z285.pdf

22. Lopato, L.M.; Shevchenko, A.V.; Kushchevskii, A.E.; Tresvyatskii, S.G. Polymorphic transformations of rare earth oxides at high temperatures. Inorganic Materials, 1974, 10(8), pp. 1276–1281.
https://www.osti.gov/biblio/4217286

23. Traverse, J.P. Study of the Polymorphism of Rare Earth Sesquioxides: These. Grenoble, 1971, 150 p. (in French).

24. Xiong, K.; Robertson, J. Electronic structure of oxygen vacancies in La_2O_3, Lu_2O_3 and $LaLuO_3$. Microelectronic Engineering, 2009, 86(7–9), pp. 1672–1675.
DOI: https://doi.org/10.1016/j.mee.2009.03.016

25. Chudinovych, O.; Zhdanyuk, N. Interaction of lanthane lutetium at temperature of 1500-1600°C. Ukrainian Chemistry Journal, 2020, 86(3), pp. 19–25. (in Ukrainian). DOI: https://doi.org/10.33609/0041-6045.86.3.2020.19-25

26. Andrievskaya, E.R. Phase equilibria in the systems of hafnium, zirconium and yttrium oxides of rare earth elements. Naukova Dumka: Kiev, 2010, 470 p. (in Ukrainian).
http://www.materials.kiev. ua/edition/13

27. Shannon, R.D. Revised effective ionic radii and systematic studies of interatomic distances in halides and chalcogenides. Acta Crystallographica Section A, 1976, 32(5), pp. 751–754.
DOI: https://doi.org/10.1107/S0567739476001551

28. Zinkevich, M. Thermodynamic Database for Rare Earth Sesquioxides. National Institute of Standards and Technology, 2007. Available online: https://materialsdata.nist.gov/handle/11256/965

29. Pavlik, A.; Ushakov, S.V.; Navrotsky, A.; Benmore, C.J.; Weber, R.J.K. Structure and thermal expansion of Lu_2O_3 and Yb_2O_3 up to the melting points. Journal of Nuclear Materials, 2017, 495, pp. 385–391.
DOI: https://doi.org/10.1016/j.jnucmat.2017.08.031

30. Axelrud, L.G.; Grin, Yu.N.; Zavaliy, P.Yu. Software Package for Structural Analysis of Crystals-CSD. General description. Lviv, 1990.
https://www.ccdc.cam.ac.uk/solutions/software/csd/

31. Chudinovych, O.V.; Bykov, O.I. Interaction of yttrium, lanthanum and erbium oxides at the temperature of 1500°C. Question of chemistry and chemical technology, 2020, 4, pp. 194–200. (in Ukrainian).
https://udhtu.edu.ua/public/userfiles/file/VHHT/2020/4/Chudinovych.pdf